Deciphering plume-lithosphere interactions beneath Europe from topographic signatures

Laurent Guillou-Frottier, Evgenii Burov, Pierre Nehlig, Robert Wyns

PII: S0921-8181(07)00059-8
DOI: doi: 10.1016/j.gloplacha.2006.10.003
Reference: GLOBAL 1254

To appear in: *Global and Planetary Change*

Received date: 25 November 2005
Accepted date: 20 October 2006

Please cite this article as: Guillou-Frottier, Laurent, Burov, Evgenii, Nehlig, Pierre, Wyns, Robert, Deciphering plume-lithosphere interactions beneath Europe from topographic signatures, *Global and Planetary Change* (2007), doi: 10.1016/j.gloplacha.2006.10.003

Deciphering plume-lithosphere interactions beneath Europe from topographic signatures

Laurent Guillou-Frottier [a,*], Evgenii Burov [b], Pierre Nehlig [a] and Robert Wyns [a]

[a] *BRGM, Orléans, France*
[b] *Université P. et M. Curie, Paris, France*

Revised manuscript submitted to *Global and Planetary Change*,
Special volume on Topography of Europe
September, 8th, 2006

[a] : BRGM, 3 av. C. Guillemin, BP 6009, 45060 Orléans Cedex 2, France; l.guillou-frottier@brgm.fr ; p.nehlig@brgm.fr ; r.wyns@brgm.fr

[b] : Laboratoire de Tectonique, Université P. et M. Curie, 4 Place Jussieu, 75252 Paris Cedex 05, France, evgenii.burov@lgs.jussieu.fr

* Corresponding author. BRGM, Service des Ressources Minérales, 3, av. C. Guillemin, BP 6009, 45060 Orléans Cedex 2, France ; fax : +33 2 38 64 36 52 ;email address : l.guillou-frottier@brgm.fr

Abstract

When a mantle plume rises and impinges on the base of the lithosphere, it expectably produces variations in surface topography. Taking into consideration a realistic mantle rheology, plume ascent rates can reach tens to hundreds of metres per year, whereupon the impingement of the plume head at the base of the lithosphere can be considered as an "impact". Recent numerical experiments based on tectonically realistic formulations for the lithosphere and a representative mantle rheology, have shown that plume-induced undulations exhibit temporal successions of uplift and subsidence at various wavelengths. From spectral (Fourier) analyses of the undulations would appear that two groups of wavelengths (200-400 km and 60-100 km) predominate. Interestingly, a spectral analysis of Europe's topography also reveals two dominant groups. In the present study, we have used a spectral analysis with a wavelet formulation in order to discriminate between tectonically-induced undulations (uni-directional deformation) and plume-induced undulations (omni-directional deformation). The European lithosphere is well-suited for this approach since it has been suggested that two mantle plumes (the Massif Central and the Eifel area) underlie Western Europe, where Alpine compression has folded the lithosphere over several hundreds of kilometres. The wavelet analysis of Europe's surface topography confirms that the energy distribution of the topographic undulations outside the two main volcanic provinces is homogeneous, thus contrasting with the coexistence of both large-scale and medium-scale high-energy features that are obtained for the Massif Central and Eifel areas. Similar signatures are also found beneath the northern Sudetes area. The wavelet approach dedicated to the analysis of plume-related topographic signatures needs, however, detailed theoretical grounds and would probably benefit from two-dimensional analyses.

Keywords: Plume; Lithosphere; Topography; Europe; Wavelet

1. Introduction

Mantle upwelling beneath western Europe has repeatedly been suggested as the main cause of Cenozoic rifting and recent volcanism (Froidevaux et al., 1974; Lucazeau et al., 1984; Granet et al., 1995; Hoernle et al., 1995; Dèzes et al., 2004), but distinct geodynamical scenarios have been proposed, from subduction-related to lower mantle plume-related upwelling (e.g. Goes et al., 1999; Michon and Merle, 2001). Several indirect methods have been used to try to decipher mantle plumes beneath continents, from geochemical analyses of erupted lavas (e.g. Peate et al., 1990; Hawkesworth et al., 2000) to geometrical studies on giant radiating dyke swarms (Ernst and Buchan, 1997). Geophysical signatures, such as gravity and geoid anomalies, and even seismic anomalies, are not easy to correlate with possible subcontinental mantle plumes, mainly because density and temperature contrasts between the possible plumes and the surrounding mantle are still debated (e.g. Goes et al., 1999; Nataf, 2000; Montelli et al., 2004; Korenaga, 2005). Surface topography has been used in the same way as geophysical data for comparing against model results, but only in the framework of oversimplified lithospheric models where rheological layering and free upper-surface boundary conditions were not accounted for (e.g. Ribe and Christensen, 1994; Sleep, 1997). Recent numerical simulations of plume-lithosphere interactions that considered a rheologically layered lithosphere with a free upper surface, have shown that topographic signatures can, in fact, provide valuable information concerning the spatial partitioning of plume-induced lithospheric strains and stresses (d'Acremont et al., 2003; Burov and Guillou-Frottier, 2005). The present study investigates the possibility of using topographic variations to decipher the presence of mantle plumes beneath Western Europe.

The topography of western Europe (which in this study is restricted to countries around the Alps) has been fully detailed by Cloetingh et al. (2005). To summarize the main causes of topography development, the authors focus on the ongoing Alpine collision and Atlantic ridge-push, while noting the possibility of mantle plumes beneath the Massif Central and Eifel-Ardennes areas (Granet et al., 1995; Sobolev et al., 1996; Ritter et al., 2001; Pilidou et al., 2005). Indeed, surface response to lithospheric deformation may be induced by both long-timescale horizontal sources (tectonics) and short time-scale vertical solicitations (mantle upwelling) and then modified by surface processes.

The above mentioned recent numerical experiments on plume-lithosphere interactions (Burov and Guillou-Frottier, 2005) have shown that within the associated topographic variations, certain wavelengths are favoured. In particular, a bimodal response clearly stands out from the power spectra of the computed surface topography at different time steps. However, even in the absence of mantle plumes, the bimodal character of surface deformation may also be observed by considering lithospheric folding and buckling processes, which are also controlled by rheological layering of the lithosphere (Burov et al., 1993). It is thus necessary to localize the source of topographic undulations before concluding to the presence of an underlying mantle plume, especially beneath Europe where Alpine compression and small-scale mantle plumes may affect surface topography. To achieve this goal, a new spectral analysis of surface topography of the European foreland is presented. It uses the wavelet approach, which enables one to discriminate between (1) the three-dimensional and spatially-restricted nature of the plume source, and (2) the two-dimensional and large-scale nature of the tectonic source.

2. Tomography and topographic signatures

Progress in seismic tomography over the last 15 years has enabled us to obtain present-day images of mantle density anomalies. As with many other continental areas, tomographic images of western Europe have mostly been interpreted as evidence of subducted slabs, probably because two-dimensional cold sheets give a better resolution (sharp and localized seismic discontinuities) than diffusive three-dimensional hot conduits. In general, the cold "blue" zones (positive density anomalies) are sharply defined in tomography, and therefore apparently easier to associate with the oceanic lithosphere; conversely, the hot "red" zones (negative density anomalies) are diffuse (blurred) and much more difficult to compare with idealized cylindrical hot conduits or mushroom-shaped plume heads. In Europe, it has been suggested that several subduction zones, or distinct subducted slabs, underlie the Pannonian Basin (Chalot-Prat and Girbacea, 2000) and the Mediterranean region (Wortel and Spakman, 1992; 2000). Because seismic tomography studies have been more focused on mantle downwelling, upwelling has often been considered as a consequence of downward flows; in other words, cold downwelling is assumed to induce adjacent upwelling. The retrograde motion of subducted slabs also tends to promote upward mantle flow. It is, however, interesting to recall that

before the spectacular success of seismic tomography around subduction zones (van der Hilst et al., 1991; Fukao et al., 1992), studies of mantle dynamics were focused more on the dynamics of mantle plumes than on subduction-related convection.

Distinct geodynamical concepts have been suggested to explain the diversity of positive and negative density anomalies in the tomographic images. In Europe, slab detachment, slab tearing, return flow induced by slab rollback, have all been proposed to explain geodynamical features, such as bimodal volcanism and the co-existence of extensional and compressional tectonic regimes. Besides, several tomography studies in the Massif Central and Eifel areas have provided fairly precise models of anomalously hot regions in the underlying mantle (Granet et al., 1995; Ritter et al., 2001). The results for both areas show vertical plume conduits (50 to 100 km wide) extending down at least to the transition zone (Ritter, 2005), although large plume heads cannot be distinguished. The possibility of detecting mantle plumes is mainly dependent on the quality of the relevant seismic data, which is subject to large variations across Western Europe. It is thus not excluded that some other European regions may also be (or have been) underlain by mantle plumes, as, for example, is suggested by geological studies in the Bohemia-Sudetes area (e.g. Crowley et al., 2000; Dostal et al., 2001).

The idea of deciphering plume-lithosphere interactions from topographic signatures has been invoked and partly tackled in Burov and Guillou-Frottier (2005). Over continents, topography data have generally been combined with gravity data to estimate mechanical properties of the lithosphere (Banks et al., 1977), and amplitudes and wavelengths of lithospheric undulations (Burov et al., 1993). The recent numerical results on plume head – continental lithosphere interactions (Burov and Guillou-Frottier, 2005) imply that surface topography may represent useful geophysical data to infer the impingement of mantle plumes at the base of the lithosphere. Actually, the associated topographic undulations may be much more complex than was previously thought, unless the continental lithosphere is thick and cratonized (in which case, a single oceanic-like domal signature is obtained). Nonetheless, despite the time-varying aspect of topographic undulations, two groups of wavelengths are promoted. Ricard et al. (1987) had already observed this bimodal character in the Basin and Range Province, and suggested that it was related to the non-linear rheology of the upper crust and the layered structure of the lithosphere. Similarly, spectral analyses of topographic signatures along the East African Rift system confirm that a bimodal signature can also be identified above mantle

plumes (Burov and Guillou-Frottier, 2005). The topographic undulations in East Africa (e.g. Morley et al., 1999) appear to be controlled by both crustal-scale and lithospheric-scale instabilities, yielding two dominant wavelength groups of around 60-100 km and 200-400 km.

As mentioned earlier, this bimodal signature can however be caused by vertical or horizontal sollicitations, and interpretations of classical (Fourier) spectral analyses are then limited. Indeed, one problem with classical spectral analysis based on the Fourier formulation is that although it allows one to determine dominant wavelengths, it remains insufficient to provide additional information such as source localization. In other words, Fourier spectral analysis cannot help in deciphering between a tectonically-induced signature and a plume-induced signature whose wavelengths would be similar. Consequently we suggest another method, which is also a spectral analysis of surface topography. Our approach is based on the wavelet technique with a “plume-specific” kernel function that allows for better deciphering of plume-like features. The selected function is formed using the analogy between the interaction of a fast plume impacting on the lithosphere, and that resulting from the fall of a droplet on a liquid interface. Since the wavelet technique enables one to localize sources of omni-directional surface undulations, it is suggested that plume-induced signatures in Europe can be deciphered and separated from those induced by the Alpine compression. With this first order approach, it is implicitely assumed that the shapes of European plumes are close to cylindrical conduits and that tectonically-induced undulations are parallel to the Alpine front.

3. Dynamic topography associated with plume-lithosphere interactions

Most of the previous analog and numerical experiments on plume-lithosphere interactions used several oversimplified assumptions that led to the concept of a thermal plume rising slowly from the base of the mantle to the lithosphere-asthenosphere boundary, where the plume head was gently flattened and spread out laterally (e.g. Griffiths and Campbell, 1991; Ribe and Christensen, 1994). Yet, when realistic mantle rheologies are considered, it appears that plume velocities are much higher than previously inferred, and that basal erosion of the mantle lithosphere is more important than was deduced from the simple models (e.g. Davies, 1994). Moreover, when appropriate surface conditions are included in the model formulation, topographic variations appear much more complex than simple

doming signatures. The two following sections describe, respectively, (1) dynamic processes associated with plume head – continental lithosphere interactions as revealed by laboratory experiments, and (2) details on dynamic topography observed in recent numerical simulations.

3.1 Plume impacting

As initially shown by Weinberg and Podladchikov (1994), rising velocities of mantle or crustal diapirs may reach tens to hundreds of metres per year, even for relatively small diapirs. Because the Stokes velocity scales as a third power of the plume head diameter, these velocities may be even higher for large plumes. The fast arrival of huge volumes of hot material at the base of the lithosphere should thus result in an "impact" on a deformable surface. Simulation of a fast thermal plume rising below a rigid continental lithosphere was performed in a laboratory experiment by Guillou and Jaupart (1995). Figure 1 shows such an experiment in which a large subcontinental plume rises intermittently. The hot material brought by the plume head is ponded beneath the continent to form a hot subcontinental layer. The regular destabilization of this subcontinental layer by the plume head gives rise to a laterally propagating undulation. However, as with this laboratory experiment, most of the previous laboratory and numerical experiments on plume-lithosphere interactions assumed a fixed (rigid) upper surface (e.g. Ribe and Christensen, 1994). If the upper surface of the laboratory model were free to deform, one can speculate that the observed undulations of the subcontinental layer (white lines in Figure 1) would be transferred (albeit in a strongly modulated form) to the upper surface. In other words, the plume head impacting the subcontinental layer could be expected to trigger significant time-varying topographic undulations at the upper surface.

Because the continental lithosphere does not behave as a single rigid (i.e. elastic) layer, the simple basal undulation suggested in Figure 1 would not have exactly the same form at the upper surface. Due to rheological layering of the lithosphere, some undulations can be expected to be attenuated and others to constructively interfere with eigen wavelengths of the lithosphere (Figure 2). In other words, the lithosphere acts as a multifrequency modulator, promoting certain wavelengths at the expense of others. Continuing with this analogy, and bearing in mind the high plume velocity, the arrival of the plume head can be considered as a Dirac pulse, whilst tectonic compression, for example, would act as a Heaviside signal, allowing for a long-term horizontal constraint. Figure 3

illustrates these two different causes of topographic undulations, and shows that they are not easily decipherable when undulations from both sources are present.

3.2 Lithospheric filter and bimodal response

Previous numerical models of plume-lithosphere interactions were generally based on solutions of viscous flow equations, and considered a plume rising below a stagnant viscous lid representing the lithosphere (Ribe and Christensen, 1994; Tackley, 2000). Moreover, in most models, the upper surface was not allowed to move vertically (fixed upper surface condition), which prevented direct calculation of the implied topography variations. Surface topography evolution in these models was roughly evaluated by assuming either local or regional (elastic flexure) isostasy. Hence, only simple large-scale surface doming was predicted, and dynamical features of the lithosphere response were ignored. Later models accounting for free surface boundary conditions and lithospheric rheology have shown that surface topography depends on several modes of lithospheric deformation, including inelastic bending, necking and faulting. The first case of such a model was presented by d'Acremont et al. (2003) who modelled surface topography evolution over an oceanic lithosphere (mono-layer). The more complex multi-layer continental lithosphere has recently been tackled by Burov and Guillou-Frottier (2005). The main results where surface topography is concerned are summarized below.

The new formulation of plume head-continental lithosphere interaction models presented in the Burov and Guillou-Frottier study (2005) includes the following improvements: (a) mantle and lithosphere rheologies no longer being limited to flow properties: elastic, viscous and plastic contributions are explicitly included in the total strain; (b) rheological layering of the crust and the lithosphere are defined by their thermal and compositional structures; and (c) a free upper surface boundary condition is allowed. The numerical code, initially developed for lithospheric deformation problems (Poliakov et al., 1993; Burov and Cloetingh, 1997), was progressively modified to tackle problems of mantle dynamics. It allows one to compute the evolution of thermal and velocity fields, effective viscosity and strain rates, rheological phases and surface topography. Initial conditions consist in fixing the initial plume diameter, the plume location and the lithospheric structure. Typical experiments include the plume's ascent through the upper mantle, its impingement on the base of the lithosphere, and the plume head spreading phase. Depending on the chosen parameters (local Rayleigh number, temperature and density contrasts, plume size), the duration of the experiments can represent up to 20 million years (m.y.) of plume-lithosphere interaction.

The main results observed in most experiments deal with the large-scale (> 500 km) and small-scale (300-400, 200-300, and 50-100 km) transient topographic signatures such as uplift and subsidence. Plume head impingement does not necessarily produce detectable large-scale doming – except in the case of a thick cold continental lithosphere – but often generates alternating small-scale surface features (basins and uplifts), which otherwise could be attributed to regional tectonics. Amplitudes of the large-scale surface uplifts turned out to be lower than those previously estimated from several studies (Monnereau et al., 1993; Davies, 1994; Cserepes et al., 2000). The initial long-wavelength surface uplift identified in the models does not exceed 800 m, and the major elevation event (1000 m) occurs at 2.5 m.y. after the onset of plume ascent. During the following evolution, middle-wavelength (<300 km) elevations of 700-800 m are progressively superimposed on the regional uplift. Then, when the mantle and crustal layers of the lithosphere are decoupled, smaller wavelengths may appear in the surface deformations. Crustal wavelengths of 50-200 km can interfere with the mantle wavelengths, which range from 50 to 1000 km depending on the mantle geotherm and rheology. This results in a much more complex topographic evolution than previously suggested from the oversimplified numerical models (see detailed comments in Burov and Guillou-Frottier, 2005). Nevertheless, at a given time step, specific wavelengths will be more present than others (see the example in Figure 4); spectral analysis of surface topography enables one to extract these more solicited wavelengths.

Such preliminary analyses have shown that two groups of wavelengths can be identified, both from the models and from the real topography variations in East Africa. The first large-wavelength group (200-400 km) corresponds to deformation related to lithospheric mantle instabilities, and the second small-wavelength group (20-80 km) reflects crustal-scale instabilities. The gap between the two groups is detected in both the real and the modelled topography. Even if absolute values of solicited wavelengths cannot be exactly compared, due to the uncertainties of model assumptions, the bimodal character of power spectra seems to represent a valid signature of plume-lithosphere interactions. However, as mentioned earlier and indicated in Figure 3, such bimodal behaviour might also be related to horizontal tectonics. Consequently, one needs a technique allowing for discrimination between the bimodal signatures of plume- and tectonically-induced deformation.

4. Recent topographic evolution of Western Europe

During the last tens of million years, the European foreland underwent a complex tectonic history. Dèzes et al. (2004) have published a series of detailed paleotectonic maps of western Europe spanning the entire Cenozoic era; they also describe the different subsequent phases of uplifts and subsidence. Evidence for lithospheric folding (e.g. Ziegler, 1990; Cloetingh et al., 2005) and for recent progressive uplifts (e.g. Garcia-Castellanos et al., 2000) enables one to consider western Europe as a natural laboratory to analyse topographic signatures in order to decipher plume-lithosphere interactions. Since our study is focused on topographic signatures lasting a few to tens of million years, only details on recent (Cenozoic) vertical motions are given below.

4.1 Uplift, rifting, subsidence

The geology of Western and Central Europe is characterized by a series of Variscan basement uplifts (Massif Central, Armorican Massif, Vosges - Black Forest Massif, Rhenish Massif and Bohemian Massif) up to several hundred kilometres in diameter and surrounded by Mesozoic and Cenozoic sedimentary formations. These large features are cut by the European Cenozoic rift system consisting of the Spanish Valencia Trough, the Gulf of Lions and the Saône, Limagne and Bresse grabens of southeastern France, the Rhine, Ruhr and Leine grabens cutting the Rhenish Shield, and the Eger graben of the Bohemian Massif.

The detailed topographic evolution of Western and Central continental Europe over the last 65 Ma is still a matter of debate (Dèzes et al., 2004). It is well constrained in places where marine deposits have been shown to occur (e.g. the Limagne Basin) or in places where continuous sedimentation allows the reconstruction of the vertical accommodation space (e.g. Paris Basin). In places of outcropping basement (e.g. Massif Central, Rhenish Massif, and Bohemian Massif), however, only fission track data and the reconstruction and dating of paleosoils and attached paleosurface isochrones enable reconstruction of the detailed vertical evolution history.

4.2 Evidence for successive vertical motions

Following Late Palaeozoic erosion, the Variscan orogenic belt disappeared below the sea and was covered by Triassic and Jurassic sediments. Parts of it were uplifted and the sedimentary cover was

eroded since the Jurassic (e.g. Netherlands) but uplift and erosion was more pervasive during the Cretaceous (Bay of Biscay Rift, southern Armorican Massif and Massif Central; Ardennes). The general uplift of the Massif Central, Rhenish Massif and Bohemian Massif is marked by a regional erosional hiatus at the Mesozoic - Cenozoic boundary.

The uplift and concomitant erosion continued in the Massif Central until the Middle Eocene when isolated and shallow depressions developed (Sissingh, 2003) with accumulation of fine-grained fluviolacustrine sediments. These depressions evolved into grabens that subsided rapidly during the Oligocene. Intermittent marine connections were established between the Alpine foreland basin and the North German Basin via the Rhone Valley and Bresse grabens and the Rhine rift system. The Rhenish Massif and the Massif Central were still located close to sea level during Oligocene times, as indicated by repeated marine incursions (Sissingh, 2003; Ziegler, 1994). During the Late Oligocene - Early Miocene, a pulse of basin inversion is evident in the Paris Basin and marks a new uplift. In the Bresse Graben, an intra-Burdigalian (18 Ma) erosional unconformity has been observed (Rocher et al., 2003) which was synchronous with northward tilting of the Massif Central, whilst in the Limagne Graben only minor fluvial deposits were deposited after Burdigalian times (Michon and Merle, 2001).

Uplift of the Vosges - Black Forest commenced at the same time (mid-Burdigalian; Laubscher, 1992) and resulted in the formation of a crustal arch with an amplitude of about 2.5 km and a wavelength of 200 km. At the Moho level, this arch forms the culmination of a broadly northeast-trending anticlinal structure that extends from the Massif Central towards the Bohemian Massif (Dèzes and Ziegler, 2002). Late Miocene inversion of the Paris Basin was synchronous with the basin's northwestward tilting and erosion of the sedimentary fill, particularly along the southeastern margin (Mégnien, 1980). At the same time, crustal extension continued across the Rhine, Roer and Hessian grabens, whilst the triple junction area of these grabens was gradually uplifted and became the site of increased volcanic activity (Sissingh, 2003). Whereas no evidence is seen for further subsidence in the Massif Central graben during the Pliocene and Quaternary, the Bresse Graben was reactivated during the Plio-Pleistocene with the deposition of up to 400 m of fluvial and lacustrine deposits. Over the last million years, the Bresse Graben has been tilted to the west, uplifted and subjected to erosion in conjunction with uplift of the entire Massif Central.

In conclusion, from the sedimentation and erosion record it is well known that tectonics in the Tertiary are marked by pulsating tectonic phases. Deformation of North western Europe is complex and resulted in many phases of basin deformation (Ziegler, 1990).

4.3 Possible horizontal and vertical causes

Cartographic synthesis of the data and paleogeodynamic reconstructions (Ziegler, 1990; Ziegler, 1994; Sissingh, 2003; Dèzes et al., 2004) show that, since the Palaeocene, the West European lithosphere has been evolving under rapidly changing stress fields reflecting changes in the interaction of the Pyrenean and Alpine orogenic belts with their forelands.

Several domal uplifts (Massif Central, Eifel area, Bohemian Massif) are associated with Tertiary - Quaternary volcanic fields. However, not all the basement uplifts are associated with magmatic activity (Armorican Massif), and volcanic activity is equally present in non-uplifted areas (Pannonian Basin). This suggests that there is no simple correlation between magmatic activity and vertical deformation of the lithosphere. The volcanic activity began during the Palaeocene, gradually increased during the Oligocene and Miocene, and is currently subactive. Seismic tomography studies (Granet et al., 1995; Ritter et al., 2001) have imaged discrete upper-mantle plumes beneath the Massif Central and the Rhenish Massif. The general thickness of the lithosphere beneath Western and Central Europe is typically 100 - 120 km, but thins to 60-80 km beneath the two main volcanic provinces (Massif Central and Rhenish Massif; Babushka and Plomerova, 2001); this has been interpreted as reflecting thermal erosion of the mantle lithosphere and as being related to mantle plumes. Note that the development of the Vosges - Black Forest arch is related to folding of the entire lithosphere, and is not associated with mantle lithospheric thinning like the Massif Central or Rhenish Massif.

5. Spectral analyses

5.1 Dominant wavelengths

Several topographic profiles in Western Europe have been extracted from the GTOPO30 database (Figure 5). The first 39 profiles are approximately perpendicular to the Alpine front, enabling folding instabilities induced by preferentially oriented compressive deformation to be easily decipherable.

Profiles 1 to 13 and 27 to 39, are focused on the Massif Central and Eifel-Ardennes areas, respectively. Profiles 52 to 54 are arcuate and approximately parallel to the Alpine front.

The left-hand column of Figure 6 shows two of these profiles that have been smoothed to retain wavelengths greater than 20 km. These profiles cross areas under which mantle plumes have been suggested (Profiles 7 over Massif Central, and Profile 34 over the Eifel area). The right-hand column shows similar profiles over the Main Ethiopian Rift area and the Tanzania Craton area in East Africa. All four profiles show small wavelength undulations (black dotted lines) superimposed on a large wavelength domal signature (grey dashed lines). The horizontal scale differs from one case to another, as would be expected for geometries of possible underlying upwelling. For example, the mantle plume beneath Tanzania may have been split by a cratonic keel into two smaller upwellings, which would thus be driven towards the craton edges (Ebinger and Sleep, 1998). The large-scale doming and the smaller-scale undulations of the four cases all reveal a bimodal signature. This bimodal character has also been observed in eastern Anatolia by Sengör et al. (2003) who got a smoothed topography similar to that revealed in East Africa.

In order to obtain quantitative results on the topographic undulations in Western Europe, the spectral content of each profile was first analysed with Fourier transforms. The power spectrum density makes it possible to depict the main topographic wavelengths, although without any information concerning the source of the undulations. Figure 7 shows the dominant wavelengths identified in two series of topographic profiles, each crossing volcanic areas. The first observation, for both series, is a clustering of small-scale wavelengths in the ~20-50 km range that is separated from a second group in the 110-150 km range. There is a clear lack of dominant wavelengths in the 50-110 km range, except for Profile 16 (see below). As identified in East Africa (Burov and Guillou-Frottier, 2005), a few spatial trends can be delineated for the largest dominant wavelengths (dotted lines). For example, the left-hand side of Figure 7 shows that the largest dominant wavelengths tend to increase from the French Massif Central to the Paris Basin area. It is not however possible to relate the identified wavelengths to a specific area since Fourier transforms use and provide features for the entire signal domain. Hence, apparent spatial trends of dominant wavelengths might not be directly attributable to a spatially varying tectonics and/or mantle dynamics.

Another piece of information comes from the amplitudes of each peak, which are represented in Figure 7 by symbol size. Large crustal wavelengths (30-50 km) show high amplitudes for profiles

crossing parts of the Massif Central (broken dotted line), Bohemia-Sudetes, and the eastern part of the Eifel-Ardennes area (encircled); the other profiles do not show these wavelengths with high amplitudes. It should be noted that the power spectrum density in the eastern part of the Eifel area shows high amplitudes for wavelengths between 35 and 54 km, unlike in the western part (see symbol sizes).

Finally, another striking result is noted out at the transition between the Massif Central area and the Eifel area, say within the Paris Basin area (left figure). With Profile 16, located between the two volcanic areas, the largest obtained wavelength is only 79 km, almost twice as small as the dominant wavelengths typically observed in the Massif Central and Eifel areas (128-146 km). As indicated by the encircled area, one can delineate an apparent spatial trend; it is as if the Massif Central and Eifel areas triggered a predominance of large-scale (150 km) wavelengths. However, as already noted above, results from Fourier transforms cannot be interpreted firmly in terms of source localization, and so it is difficult to proceed further in our interpretation of the results. In order to squeeze even more information from the topographic profiles, we have refined our spectral analyses using the wavelet method. As explained below, this method provides additional information from topographic undulations and facilitates the deciphering of omni-directional plume-related signatures from directional tectonic signatures.

5.2 Wavelet formulation for topographic signatures

In addition to the classical Fourier transform, which is most efficient for infinite periodic signals, harmonic analysis also deals with other closely related, but more specialized, integral transforms, many of which are based on convolution with custom-tuned signal-specific kernel functions. In particular, the wavelet transform provides a choice of kernel functions (or “mother wavelets”) that are particularly well adapted for the analysis of localized three-dimensional features.

There are several advantages of using the wavelet method for spectral analysis of topographic profiles. First, as is well-known (e.g. Meyer, 1992), this method enables one to spatially localize the source of undulations. Second, the plume-related signatures, which largely resemble a droplet on a liquid interface (Figure 8), show a good fit with the shape of some of typical wavelet functions; this, for example, is the case of the typical "Morlet" curve, used as one of the mother wavelet functions (see below). Third, depending on what it is being sought, one can use different mother wavelets and thus

decipher different temporarily defined snapshots of plume-lithosphere interactions. As shown in Figure 3, surface signatures differ from one time step to another, so that present-day surface signatures may contain vanishing phases of plume-lithosphere interactions (e.g. a plume impinging the European lithosphere 20 m.y. ago) as well as the recent ones (present-day plume impacting).

Unlike the spectral techniques based on the Fourier transform, the wavelet technique allows one to examine each spectral component locally. Localization is obtained by comparing (convoluting) the input signal with a specific kernel function called wavelet. The wavelet parameters (two coefficients *a* and *b*) are varied in order to span the range of possible locations and frequencies (Meyer, 1992; Gaillot, 2000). Continuous wavelet transform of surface topography *h*(*x*) can be defined as:

$$C_h(a,b) = \int h(t)\ \overline{y}_{a,b}(t)\ dt \qquad (1)$$

where *a*>0, and where $\overline{y}$ is the conjugate of y, the ("mother") wavelet, which defines a series of functions:

$$y_{a,b}(t) = \frac{1}{\sqrt{a}}\, y\left(\frac{t-b}{a}\right) \qquad (2)$$

where *a* is the scale (or dilatation) parameter and *b* the position (or translation) parameter.

The wavelet coefficients $C_h(a,b)$, given by equation (1), contain all the necessary information for a multi-scale analysis. Their values increase as the shape of the analysed signal approaches the shape of the wavelet. Several types of "mother wavelet" can be used, depending on what is being sought within the signal, but they must all obey mathematical properties such as a zero mean value, a fast decay towards zero at the sides, etc. The mother wavelets most frequently used in geophysics are the "Mexican hat" curve - as well as other variants of a Gaussian function - and the Morlet wavelet (Figure 8).

The "Mexican hat" wavelet is simply the negative of the second derivative of the Gaussian distribution, taking the form:

$$y_{MH}(x) = \frac{1}{\sqrt{2p}}(1-x^2)\, e^{-x^2/2} \qquad (3)$$

This mother wavelet was used by Malamud and Turcotte (2001) and by Turcotte et al. (2002) to estimate crustal and lithospheric thicknesses on Mars, and by Vecsey et al. (2003) to detect tectonic features in geoid signals.

The Morlet wavelet (Grossman and Morlet, 1984) is defined as:

$$y_{MO}(x) = p^{-1/4} e^{iw_0 x} e^{\left(-\frac{x^2}{2}\right)} \quad (4)$$

where x is the distance, and w_0 is the wave number. This mother wavelet was used by Little et al. (1993) to decipher a low-frequency zone in bathymetric profiles northeast of Hawaï, and by Gaillot (2000) to study climatic and paleomagnetic signals. The wavelet is defined on a complex space (real and imaginary (phase) part), and thus allows one to use phase analysis to obtain additional information on the signal. When a signal is supposed to show an oscillatory behaviour, it is better to choose a complex mother wavelet, such as the Morlet wavelet, whereas a real (non complex) mother wavelet can be used to isolate peaks or discontinuities in the signal (Torrence and Compo, 1998).

Because we are interested in localized three-dimensional signatures as well as in two-dimensional undulations, we performed spectral analyses with both types of mother wavelet.

Continuous wavelet transforms of topography h(x), i.e. coefficients $C_h(a,b)$, can be illustrated by scalograms, where the horizontal axis stands for the position parameter (b) and the vertical axis for the dilatation parameter (a). The scalogram refers to an energy distribution defined as the square modulus of the wavelet coefficients. Coefficient values are represented by different colours, with the brighter colours indicating the higher coefficient values (i.e. a closer match with the signal). In the case of a bidimensional mono-wavelength folding of the lithosphere, one would expect a scalogram containing regular patterns (similar high coefficient values at the same scale) all along the horizontal axis, but for a three-dimensional spatially restricted signature, such as that due to plume-lithosphere interaction, one would expect only localized high-energy coefficients. In our experiments, the tests on numerical profiles were made with the scale parameter a ranging from 1 to 100, but for the real topographic profiles whose lengths are two to four times smaller, scalograms with a values ranging from 1 to 50 were sufficiently different to discriminate between distinct signatures. Where high-energy coefficients are identified, we have qualified them as "medium-scale" for a values around 20-30, and "large-scale" for coefficients above ~30.

5.3 Numerical profiles

Before analysing real topographic profiles, we performed continuous wavelet transforms of a computed topography predicted from the numerical experiments on plume-lithosphere interaction. The

two cases shown in Figures 9a and 9b (first rows) correspond to distinct dynamic regimes, which can be parameterized by a plume Rayleigh number Ra_p (see details in Burov and Guillou-Frottier, 2005). The chosen dynamical regimes in Figure 9 correspond to the most commonly accepted convective regimes in the Earth's mantle. In the first case (Figure 9a, $Ra_p = 10^6$), surface topography (second row) evolves from a single large-scale doming signature (time step of 0.6 m.y.) towards an undulating signature (2.4 m.y.) and ends with additional uplift signatures due to the arrival of secondary upwelling (10 m.y.). The second case occurs with a more turbulent convective regime (Figure 9b, $Ra_p = 5.10^6$), where secondary plumes are already rising 1 m.y. after the onset of the experiment. Surface topography thus exhibits several plume-related undulations. Wavelet transforms (third and fourth rows) were performed with both "Mexican hat" and Morlet wavelets.

As can be seen, a variety of scalograms was obtained, and several points need to be emphasized. First, when the topography produced by a single plume is analysed (case of $Ra_p=10^6$, Figure 9a, at time steps 0.6, 2.4 and 5.5 m.y.), the "Mexican hat" wavelet seems more appropriate than the Morlet wavelet for illustrating and localizing the energetics of the plume. The Morlet wavelet could also be used, but not for the initial stage. Moreover, signatures obtained at the extreme edges of each scalogram are not necessarily related to the analysed signal, (Gaillot, 2000). Second, when the upwelling dynamics is much more active ($Ra_p=5\ 10^6$, Figure 9b), scalograms obtained with the Morlet wavelet (hereafter called "MO scalograms") do not seem to either localize or distinguish between the plume features. Conversely, scalograms obtained with the "Mexican hat" wavelet (hereafter called "MH scalograms") allow one to separate plume conduits from the large plume head (see time steps 1.5 and 4.4 m.y.). Thus two distinct signatures are visible on the MH scalograms of Figure 9b; several medium-scale high-energy coefficients (white ellipses) and one large-scale high-energy peak. More precisely, the scale involved by plume-conduit solicitations is about half that imaged below plume heads. When convective mixing is achieved (time step 11 m.y.), the single high-energy feature on scalogram refers to the largest upwelling structure from the bottom to the top of the model (right part of the box). Third, as is well-known (e.g. Meyer, 1992) the "Mexican hat" wavelet has the same ability to decipher mono-wavelength undulations as the Morlet wavelet. In other words, undulations induced by tectonic stresses would be imaged by both mother wavelets, but plume-induced signatures may not be easily decipherable with the Morlet wavelet.

5.4 Profiles from Western Europe

Figure 10a and 10b show continuous wavelet transforms of topographic profiles between the Massif Central and the Eifel areas (Profiles 14 to 18) and outside the topography highs (Profile 52). Profiles 14 to 18 begin at the western edge of the Alps and are parallel to the Alpine compression. The MH scalograms show no small-scale high-energy coefficients, only large-scale high-energy peaks (Figure 10a). A regular pattern (with a wavelength of ~200-250 km) clearly appears in Profiles 15 to 18. The wavelet transform of Profile 14 appears dominated by the nearby Massif Central signal. Some small-scale medium-energy features are obtained in Profiles 17 and 18 (see white ellipses), but are not visible in Profiles 14 to 16. As expected, the MO scalograms are more difficult to interpret, but for Profiles 17 and 18, closest to the Eifel area, the high-energy coefficients resemble the numerical case of Figure 9b, where both small-scale and large-scale high-energy features are obtained. It must be noted that the small-scale high-energy peaks in the MO scalogram of Profile 18 correspond to the western edge of the Eifel-Ardennes topographic high.

Profile 52 bypasses the topographic highs and crosses the Paris and North German basins. The associated MH scalogram (Figure 10b) emphasizes, with a three-dimensional view, the homogeneous energy distribution of the topographic undulations (apart from edge effects). The largest energy coefficients appear to be regularly spaced with an apparent horizontal wavelength of ~100 km. The two other arcuate profiles (Profiles 53 and 54) were also analysed (Figure 11). Profile 53 crosses the Massif Central, the Paris Basin, the Eifel area and the northern Sudetes; Profile 54 crosses the Massif Central, the south of the Eifel area (Rhine Graben) and central Bohemia. Several interesting features appear in the three-dimensional views of Figure 11: (1) high-energy coefficients (6 times greater than in Figure 10b) at both medium and large scales are imaged below the Massif Central; (2) the Eifel area shows the same characteristics (but with a smaller energy) in the case of Profile 53; (3) Profile 53 also reveals high-energy coefficients in the northern Sudetes area; (4) the Rhine Graben (Profile 54) exhibits medium-scale high-energy coefficients, but no large-scale ones; (5) high-energy coefficients below the Bohemia area could confirm the Sudetes trend, but could also be attributed to border-effects.

5.5 A closer look at supposed mantle plumes

As mentioned earlier, a mantle-plume induced undulation is assumed to show approximately similar scalograms in all directions. The presence of both medium- and large-scale high-energy coefficients in

the scalograms above the Massif Central and Eifel-Ardennes areas (Figure 11) thus needs to be confirmed from distinct topographic profiles. A series of east-west topographic profiles crossing the Massif Central from south to north (Profiles 1 to 13), and a series of southwest-northeast topographic profiles crossing the Eifel area (Profiles 27 to 39) were analysed with the same continuous wavelet transform technique as above.

Figure 12 shows topographic profiles across the Massif Central (without the Alps) in the left-hand column and the equivalent continuous wavelet transforms in the right-hand column. The "Mexican hat" wavelet was used in order to decipher the presence of both medium- and large-scale high-energy coefficients more easily. Profiles 2, 4 and 13 have been removed because their scalograms are similar to those of their adjacent profiles. Medium-scale high-energy coefficients are clearly present on Profiles 7 to 11 (white ellipses), representing the northern part of the Massif Central. From south to north, one also observes that the large-scale high-energy coefficients split regularly in two parts, separated by an apparent medium-scale high-energy feature becoming increasingly present.

Figure 13, for the Eifel-Ardennes area, shows medium-scale medium-energy coefficients on Profiles 32 to 36 (white ellipses). In Profiles 37 to 39, these medium-scale medium-energy coefficients disconnect from the large-scale high-energy feature, and tend to disappear. In Profiles 32 to 35, a second group of large-scale medium-energy coefficients appears to the northwest of the predominant feature.

Finally, wavelet transforms were also performed on topographic Profiles 22 to 26 (Sudetes-Bohemia area) in order to validate, or otherwise, the apparent plume-like features identified with Profiles 53 and 54. Profiles 22 to 26 are perpendicular to Profiles 53 and 54, and thus plume-like signatures, if they exist, should be identified at the same location as that revealed in Figure 11. Figure 14 illustrates medium-scale medium-energy coefficients for the easternmost Profiles 25 and 26 (white ellipses). Hence, the plume-like feature identified in the left-hand scalogram of Figure 11, corresponding to eastern part of Profile 53 (Sudetes area), appears to be confirmed by the emergence of these medium-scale medium-energy coefficients. On the other hand, the high-energy peak of the right-hand scalogram of Figure 11 (Bohemia area) is not clearly supported by the medium-scale medium-energy coefficients in Figure 14.; the peak in Figure 11 might thus be due to border effects.

6. Discussion and conclusion

6.1 Wavelet, topography and plumes

The evolution of surface topography results from both long-term geodynamic processes lasting tens to hundreds of m.y., such as tectonic compression, and short-term external solicitations of a few m.y., such as erosion. Similarly, the impingement of a mantle plume at the base of the continental lithosphere involves both long-term and short-term lithospheric undulations. Large-scale doming signatures of several hundreds of kilometres related to active mantle plumes could be considered as permanent (e.g. the Afar doming; Sengör, 2001; examples in Figure 6), but in some cases, specifically if the plume becomes detached from its conduit, small-scale uplift and subsidence of several tens of kilometres may overprint or destroy the long-wavelength signatures within a few m.y. (e.g. examples in Figure 9; Burov and Guillou-Frottier, 2005). Nevertheless, as suggested from spectral analyses, plume-induced signatures appear to be particularly unique in that they are locally restricted, mainly axi-symmetric, and resemble typical wavelet functions (Figure 8). Wavelet transforms of surface topography reveal that the energy distribution is homogeneous away from areas of supposed mantle plumes (Figures 10a and 10b) whereas a bimodal character is obtained for profiles crossing the Massif Central and Eifel areas (Figures 11 to 13), and possibly the northern Sudetes area (Figure 14). As suggested by scalograms of computed topographic profiles, large-scale high-energy coefficients may be related to plume heads, and medium-scale high-energy coefficients may be promoted by plume conduits (Figure 9b). Such preliminary interpretations clearly require further investigations, especially where previous results from Fourier spectral analyses have to be considered —the bimodal character inferred from Fourier spectral analyses was associated with lithospheric and crustal wavelengths, whereas the bimodal character in wavelet scalograms may be related to plume heads and conduits. It must be emphasized that this latter interpretation has the advantage of taking into account the localization property of the wavelet transform.

As mentioned earlier, this study does not consider previous models where complex shapes of European upwellings were proposed (e.g. Goes et al., 1999). Nonetheles, numerical simulations were actually performed in a two-dimensional frame, allowing the concept of an upwelling sheet (thus perpendicular to plane views) to be accounted for. Similarly, the hypothesis of homogeneous folding instabilities induced by tectonic compression (Figure 3a) might be questioned if pre-existing local

heterogeneities are considered. However, scalograms of Figures 10 and 11 (outside topographic highs, and in perpendicular directions) strictly differ from those crossing Massif Central and Eifel areas, Indeed, the absence of medium-scale high-energy coefficient for Profiles 14 to 16 and the absence of large-scale high-energy coefficients for Profile 52, justify the need of analysing topographic profiles in at least two directions. It must be noted that the method presented in this study was recently applied to east Africa (Guillou-Frottier and Burov, 2006). Similar wavelet signatures (same specific scalograms) were also obtained over areas where recent tomography results (Weeraratne et al., 2003) strongly suggest the presence of an upper mantle plume.

6.2 4D topography evolution in Europe

The first results obtained in this study reveal that parts of the considered European topographic profiles are associated with specific wavelet signatures similar to those obtained in numerical simulations of plume-lithosphere interaction. However, the analogy between numerical and real profiles has to be considered with care, because a number of hypotheses in numerical experiments (e.g. flat geometry for the lithosphere-asthenosphere boundary, thermal age of the lithosphere, size of rising plume, etc.) can affect the topographic signature. Although some of these effects have been described in Burov and Guillou-Frottier (2005), the experiments chosen for this study (Figure 9) correspond to realistic thermal and mechanical regimes of the European lithosphere (Cloetingh et al., 2005), as well as to realistic convective regimes (Guillou and Jaupart, 1995). Moreover, the size of the plumes rising beneath Europe may be smaller than that imposed in the experiments of Figure 9 (see below), which would actually reinforce the consequences in terms of topographic undulations (see Figure 10 in Burov and Guillou-Frottier, 2005, that show a clear bimodal character).

The topography of Europe has evolved significantly over the last tens of million years, with several phases of uplift and subsidence (see Section 4). Successive vertical motions, such as basin inversions, could be related to intermittently rising mantle plumes (e.g. Figure 1), which are typical of convective regimes at high Rayleigh numbers (case of Figure 9b). In East Africa, multiple phases of tectonic inversion have been shown to occur over a relatively short period (Morley et al., 1999), and rift basins of the northern Kenyan rift were only active for a few million years (Morley et al., 1992). These short time-scale events are difficult to reconcile with tectonically-induced stresses, which persist over several tens to hundreds of m.y. (e.g. Cloetingh et al., 1999). Even though volcanism does not

necessarily occur above mantle plumes, the presence of Tertiary-Quaternary volcanic fields above uplifted areas (Massif Central, Eifel area and Bohemian Massif), the apparent thermo-mechanical weakening under the Massif Central and Eifel area (Granet et al., 1995; Garcia-Castellanos et al., 2000) and evidence of successive vertical motions, are sufficiently convincing factors with which to attempt to decipher possible mantle plumes from topographic signatures.

However, it must be emphasized that several other mechanisms play a significant role in the 4D topography evolution, but not necessarily at similar wavelengths as those triggered by mantle plumes. Surface erosion processes (e.g. fluvial erosion, leading for example to large river valleys – or sedimentation), tend to localize - or smooth - topographic amplitudes, but they will not modify the pre-existing wavelengths created by deeper processes. Tectonic inversion and similar vertical crustal motions cannot be compared with omnidirectional topographic undulations typical of plume-induced topography. Indeed, the faults associated with a major deformation (tectonically- or plume-induced) do not create new wavelengths, and can only slightly change the wavelength of the initial deformation. In addition, all these important mechanisms (erosion, sedimentation, vertical crustal motions) primarily affect small (< 50 km) wavelengths and are less effective on large ones. Consequently, topographic signatures associated with mantle plume impacting should not be obscured neither removed by other small-scale and spatially restricted mechanisms.

Tomography studies in the Massif Central and Eifel areas (Granet et al., 1995; Ritter et al., 2001; Ritter, 2005) do not allow to clearly distinguish large plume heads. This may be related to the age of the European plumes (important thermal diffusion), considering that the main initial uplift would have started at more than 60 Ma for the Massif Central and more than 30 Ma for the Eifel-Ardennes area (Garcia-Castellanos et al., 2000). This would imply that domal uplift, as represented in Figures 6 and 8e, corresponds to frozen undulations kept in lithospheric memory, whereas small-scale wavelengths would be related to more recent dynamic signals, such as fast rising mantle batches through plume conduits. Such a scenario would be compatible with the global tomography results of Goes et al. (1999) and with the small-scale plume concept described by Ritter (2005). The apparent plume signature inferred beneath the Sudetes (Figure 14) would also reinforce the initial suggestion by Granet et al. (1995).

The wavelet transforms of European surface topography have shown that both large-scale and medium-scale high-energy coefficients are present beneath areas of supposed mantle plumes,

whereas a homogeneous energy distribution is obtained outside. Thanks to lithosphere's memory of large-scale uplifts, this new approach would appear to be useful in distinguishing between tectonically-induced undulations (homogeneous distribution of high-energy coefficients outside topographic highs) and plume-induced undulations (presence of both large-scale and medium-scale high-energy coefficients beneath the Massif Central, Eifel and Sudetes areas). A number of theoretical improvements are, however, necessary before tackling a more rigorous study of plume-induced topographic signatures.

6.3 Further studies

This study was not dedicated to finding a best mother wavelet for depicting plume-related features. However, as explained in Section 5.2, the choice of the best adapted mother wavelet appears to be critical. The analysis of scalogram differences given in Figure 9 shows that transient features of surface topography may not be as easily decipherable with the Morlet wavelet as with the "Mexican hat" wavelet. This preliminary observation is not, however, necessarily valid for the ocean floor topography where less "plate" filtering is expected because of a simpler thermo-mechanical lithospheric structure. Similarly, a specific mother wavelet may or may not be efficient, depending on the local thermo-mechanical regime of the continental lithosphere. Moreover, when studying plume-lithosphere interactions, changes in the rheological structure of the lithosphere, as suggested for Europe by Cloetingh and Van Wees (2005), may be seen after only a few tens of m.y.; this will require re-adjustment of the mother wavelets between the initial plume ascent stage and the steady-state rise of mantle material through an already emplaced plume conduit. The approach clearly needs further investigation closely related to the geological contexts of the studied areas.

The next step in developing this approach should be a two-dimensional analysis of surface topography, as was done for Fourier transforms by Ricard et al. (1987). This would be especially useful because plume-induced topographic undulations are locally restricted and tend to exhibit concentric symmetry (Garcia-Castellanos et al., 2000). Once possible specific wavelets adapted to plume signatures have been defined, then the method should be tested on other well-known subcontinental mantle plumes.

Acknowledgments

We would like to thank reviewers J. Van Wijk and J-D. van Wees for useful comments and advice which help to improve our paper. We also thank the BRGM Translation unit for proofreading the manuscript. This is BRGM contribution no. 4059.

References

d'Acremont, E., Leroy, S., Burov, E.B., 2003. Numerical modelling of a mantle plume : the plume head-lithosphere interaction in the formation of an oceanic large igneous province. Earth Planet. Sci. Lett., 206, 379-396.

d'Agostino, N., Jackson, J.A., Dramis, F., Funiciello, R., 2001. Interactions between mantle upwelling, drainage evolution and active normal faulting : an exemple from the central Appennines (Italy). Geophys. J. Int., 147, 475-497.

Babushka, V., Plomerova, J., 2001. Subcrustal lithosphere around the Saxothurangian-Moldanubian suture zone – a model derived from anisotropy of seismic wave velocities. Tectonophysics, 332, 185-199.

Banks, R.J., Parker, R.L., Huestis, S.P., 1977. Isostatic compensation on a continental scale : local versus regional mechanisms. Geophys. J. R. astr. Soc., 51, 431-452.

Burov, E.B., Cloetingh, S., 1997. Erosion and rift dynamics: new thermo-mechanical aspects of post-rift evolution of extensional basins. Earth Planet. Sci. Lett., 150, 7–26.

Burov, E., Guillou-Frottier, L., 2005. The plume head-continental lithosphere interaction using a tectonically realistic formulation for the lithosphere. Geophys. J. Int., 161, 469-490.

Burov, E.B., Lobkovsky, L.I., Cloetingh, S., Nikishin, A.M., 1993. Continental lithosphere folding in central Asia (part II) : constraints from gravity and topography. Tectonophysics, 226, 73-88.

Chalot-Prat, F., Girbacea, R., 2000. Partial delamination of continental mantle lithosphere, uplift-related crust±mantle decoupling, volcanism and basin formation: a new model for the Pliocene±Quaternary evolution of the southern East-Carpathians, Romania. Tectonophysics, 327, 83-107.

Cloetingh, S., Burov, E., Poliakov, A., 1999. Lithosphere folding: primary response to compression ? (from central Asia to Paris basin). Tectonics, 18, 1064-1083.

Cloetingh, S., Ziegler, P.A., Beekman, F., Andriessen, P.A.M., Matenco, L., Bada, G., Garcia-Castellanos, D., Hardebol, N., Dèzes, P., Sokoutis, D., 2005. Lithospheric memory, state of stress and rheology :neotectonic controls on Europe's intraplate continental topography. Quatern. Sci. Rev., 24, 241-304.

Crowley, Q.G., Floyd, P.A., Winchester, J.A., Franke, W., Holland, J.G., 2000. Early Palaeozoic rift-related magmatism in Variscan Europe : fragmentation of the Armorican Terrane Assemblage. Terra Nova, 12, 171-180.

Cserepes, L., Christensen, U.R., Ribe, N., 2000. Geoid height versus topography for a plume model of the Hawaian swell. Earth Planet. Sci. Lett., 178, 29-38.

Davies, G.F., 1994. Thermomechanical erosion of the lithosphere by mantle plumes. J. Geophys. Res., 99, 15709-15722.

Dèzes, P., Ziegler, P.A., 2002. Map of the European Moho. http://www.unibas.ch/eucor-urgent.

Dèzes, P., Schmid, S.M., Ziegler, P.A., 2004. Evolution of the European Cenozoic Rift System: interaction of the Alpine and Pyrenean orogens with their foreland lithosphere. Tectonophysics, 389, 1-33.

Doin, M-P., Fleitout, L., Christensen, U., 1997. Mantle convection and stability of depleted and undepleted continental lithosphere. J. Geophys. Res., 102, 2771-2787.

Dostal, J., Patoka, F., Pin, C., 2001. Middle/late Cambrian intracontinental rifting in the central West Sudetes, NE Bohemian Massif (Czech Republic) : geochemistry and petrogenesis of the bimodal metavolcanic rocks. Geol. J., 36, 1-17.

Ebinger, C., Sleep, N., 1998. Cenozoic magmatism in central and east Africa resulting from impact of a one large plume. Nature, 395, 788-791.

Ernst, R.E., Buchan K.L., 1997. Giant radiating dyke swarms: their use in identifying pre-Mesozoic large igneous provinces and mantle plumes. In: Mahoney, J., Coffin, M. (Eds.), Large Igneous Provinces: Continental, Oceanic, and Planetary Volcanism. AGU Geophys. Monogr. Ser. 100, pp. 297-333.

Froidevaux C., Brousse, R., Bellon, H., 1974. Hot spot in France ?. Nature, 248, 749-751.

Fukao, Y., Obayashi, M., Inoue, H., and Nenbai, M., 1992. Subducting slabs stagnant in the transition zone. J. Geophys. Res., 97, 4809-4822.

Gaillot, P., 2000. Ondelettes continues en Sciences de la Terre – méthodes et applications. PhD thesis, Université de Toulouse III, France.

Garcia-Castellanos, D., Cloetingh, S., van Balen, R., 2000. Modelling the middle Pleistocene uplift in the Ardennes-Rhenish massif : thermo-mechanical weakening under the Eifel ?. Glob. Planet. Change, 27, 39-52.

Goes, S., Spakman, W., Bijwaard, H., 1999. A lower mantle source for central european volcanism. Science, 286, 1928-1931.

Granet, M., Wilson, M., Achauer, U., 1995. Imaging a mantle plume beneath the French Massif Central. Earth Planet. Sci. Lett., 136, 281-296.

Griffiths, R.W., Campbell, I.H., 1991. Interaction of mantle plume heads with the Earth's surface and onset of small-scale convection. J. Geophys. Res., 96, 18295-18310.

Grossmann, A., Morlet, J., 1984. Decomposition of Hardy functions into square integrable wavelets of constant shape. SIAM J. Math. Anal., 15, 723-736.

Guillou, L., Jaupart, C., 1995. On the effects of continents on mantle convection. J. Geophys. Res., 100, 24217-24238.

Guillou-Frottier, L., Burov, E., 2006. Wavelet analyses of surface topography in east Africa: the mantle plume signatures, European Geosciences Union meeting, Geophys. Res. Abstr., 8, 06658.

Hawkesworth, C.J., Gallagher, K., Kirstein, L., Mantovani, M., Peate, D., Turner, S., 2000. Tectonic controls on flood basalt magmatism in the Parana-Etendeka Province. Earth Planet. Sci. Lett. 179, 335-349.

Hoernle, K., Zhang, Y.-S., Graham, D., 1995. Seismic and geochemical evidence for large-scale mantle upwelling beneath the eastern Atlantic and western and central Europe. Nature, 374, 34-39.

Korenaga, J., 2005. Firm mantle plumes and the nature of the core-mantle boundary region, Earth Planet. Sci. Lett. 232, 29-37.

Kumar, P., Foufoula-Georgiou, E., 1997. Wavelet analysis for geophysical applications, Rev. Geophys., 35, 385-412.

Laubscher, H., 1992. Jura kinematics and the Molasse Basin. Eclogae Geol. Helv., 85, 653-675.

Little, S. A., Carter, P.H., Smith, D.K., 1993. Wavelet analysis of a bathymetric profile reveals anomalous crust. Geophys. Res. Lett., 20, 1915-1918.

Lucazeau, F., Vasseur, G., Bayer, R., 1984. Interpretation of heat flow data in the French Massif Central. Tectonophysics, 103, 99-119.

Malamud, B.D., Turcotte, D.L., 2001. Wavelet analysis of Mars polar topography. J. Geophys. Res., 106, 17497-17504.

Mégnien, C., 1980. Synthèse géologique du Bassin de Paris. Mémoires du BRGM n° 102, 1980.

Meyer, Y., 1992. Wavelet and operators, Cambridge University Press, New York.

Michon, L., Merle, O., 2001. The evolution of the Massif Central rift : spatio-temporal distribution of the volcanism. Bull. Soc. Geol. Fr., 172, 2, 69-80.

Monnereau, M., Rabinowicz, M., Arquis, E., 1993. Mechanical erosion and reheating of the lithosphere: a numerical model for hotspots swells. J. Geophys. Res., 98, 809-823.

Montelli, R., Nolet, G., Dahlen, F.A., Masters, G., Engdahl, E.R., Hung, S.H., 2004. Finite-frequency tomography reveals a variety of plume in the mantle. Science, 303, 338-343.

Morley, C.K., Wescott, W.A., Stone, D.M., Harper, R.M., Wigger, S.T., Karanja, F.M., 1992. Tectonic evolution of the northern Kenyan rift. J Geol. Soc. London, 149, 333-348.

Morley, C.K., Harper, R.M., Wigger, S.T., 1999. Tectonic inversion in east Africa. In : Morley, C.K. (ed.), Geoscience of Rift Systems – Evolution of East Africa, AAPG Studies in Geology, 44, pp193-210.

Nataf, H.-C., 2000. Seismic imaging of mantle plumes. Ann. Rev. Earth Planet. Sci., 28, 391-417.

Parsons, B., Sclater, J. G., 1977. An analysis of the variation of ocean floor bathymetry and heat flow with age. J. Geophys. Res., 82, 803-827.

Peate, D. W., Hawkesworth, C.J., Mantovani, M.S.M., Shukowsky, W., 1990. Mantle plumes and flood-basalt stratigraphy in the Parana, South America. Geology, 18, 1223-1226.

Pilidou, S., Priestley, K., Debayle, E., Gudmundsson, O., 2005. Rayleigh wave tomography in the north Atlantic : high resolution images of the Iceland, Azores and Eifel mantle plumes. Lithos, 79, 453-474.

Poliakov, A.N.B., Cundall, P., Podlachikov, Y., Laykhovsky, V., 1993. An explicit inertial method for the simulation of visco-elastic flow: an evaluation of elastic effects on diapiric flow in two- and three-layers models. In: Stone, D.B., Runcorn S.K. (Eds), Flow and Creep in the Solar System: Observations, Modelling and Theory, Dynamic Modelling and Flow in the Earth and Planets. Kluwer, Holland, pp.175-195.

Ribe, N.M., Christensen, U.R., 1994. Three-dimensional modeling of plume-lithosphere interaction. J. Geophys. Res., 99, 669-682.

Ricard, Y., Froidevaux, C., Simpson, R., 1987. Spectral analysis of topography and gravity in the Basin and Range Province. Tectonophysics, 133, 175-179.

Ritter, J.R.R., 2005. Small-scale mantle plumes : imaging and geodynamic aspects. In Wenzel, F. (ed.), Perspectives in modern seismology. Lecture notes in Earth Sciences, 105, Springer Verlag, Heidelberg, Germany, pp. 69-94, 2005.

Ritter, J.R.R., Jordan, M., Christensen, U.R., Achauer, U., 2001. A mantle plume below the Eifel volcanic fields, Germany. Earth Planet. Sci. Lett., 186, 7-14.

Rocher, M., Chevalier, F., Petit, C., Guiraud, M., 2003. Tectonics of the northern Bresse region (France) during the Alpine cycle. Geodyn. Acta, 16, 131-147.

Sengör, A.M.C., Ozeren, S., Zor, E., Genc, T., 2003. East Anatolian high plateau as a mantle-supported, N-S shortened domal structure. Geophys. Res. Lett., 30, 8045, doi:10.1029/2003GL017858.

Sengör, A.M.C., 2001. Elevation as indicator of mantle-plume activity. Geol. Soc. Am. Sp. Pap., 352, 183-225.

Sissingh, W., 2003. Tertiary paleogeographic and tectonostratigraphic evolution of the Rhenish triple junction. Palaeogeogr. Palaeoclimatol. Palaeoecol., 196, 229-263.

Sleep, N., 1997. Lateral flow and ponding of starting plume material. J. Geophys. Res., 102, 10001-10012.

Sobolev, S.V., Zeyen, H., Stoll, G., Werling, F., Altherr, R., Fuchs, K., 1996. Upper mantle temperatures from teleseismic tomography of French Massif Central including effects of composition, mineral reactions, anharmonicity, anelasticity and partial melt. Earth Planet. Sci. Lett., 139, 147-163.

Tackley, P.J., 2000. Mantle convection and plate tectonics; toward an integrated physical and chemical theory. Science, 288, 2002-2007.

Torrence, C., Compo, G., 1998. A practical guide to wavelet analysis. Bull. Amer. Meteorol.Soc., 79, 61-78.

Turcotte, D.L., Shcherbakov, R., Malamud, B.D., Kucinskas, A.B., 2002. Is the Martian crust also the Martian lithosphere ?. J. Geophys. Res., 107, E11, 5091.

van der Hilst, R., Engdahl, E.R., Spakman, W., and Nolet, G., 1991. Tomographic imaging of subducted lithosphere below northwest Pacific island arcs. Nature, 357, 37-43.

Vecsey, L., Hier Majumder, C.A., Yuen, D.A., 2003. Multiresolution tectonic features over the Earth inferred from a wavelet transformed geoid. Vis. Geosci., 8, 26-44.

Weeraratne, D.S., Forsyth, D.W., Fisher, K.M., Nyblade, A.A., 2003. Evidence for an upper mantle plume beneath the Tanzanian craton from Rayleigh wave tomography, J. Geophys. Res., 108(B9), 2427.

Weinberg, R.F., Podladchikov, Y., 1994. Diapiric ascent of magmas through power-law crust and mantle. J. Geophys. Res., 99, 9543-9559.

Wortel, M.J., Spakman, W., 2000. Subduction and slab detachment in the Mediterranean-Carpathian region. Science, 290, 1910-1917.

Wyns, R., Quesnel, F., Simon-Coinçon, R., Guillocheau, F., and Lacquement, F., 2003. Major weathering in France related to lithospheric deformation. Géologie de la France, 1, 79-87.

Ziegler, 1990. Geological Atlas of Western and Central Europe, Shell internat. Petrol. Mij., Dist. Geol. Soc. Publ. House, Bath, 2nd ed. 239 pp. and 56 encl.

Ziegler, P.A., 1994. Cenozoic rift system of western and central Europe : an overview. Geol. Mijnb., 73, 99-127.

Figure captions

Figure 1: Laboratory experiment on plume-lithosphere interaction beneath a continent, using an imposed Rayleigh number of 1.8 10^6, where the heterogeneous thermal condition at the upper surface accounts for the insulating behaviour of continents. Here, the fluid is Newtonian and the upper surface is fixed (see details on experimental procedure and set-up in Guillou and Jaupart, 1995). The pictures are shadowgraphs of the same experiment at successive time steps. The black horizontal lines are shadows of immersed temperature probes. The white zones represent downwelling (cold zones) and the black zones upwelling (hot zones). A large thermal plume is centred beneath the continent. At the upper surface, the hot subcontinental layer is intermittently fed by the plume head, giving rise to transient undulations of the subcontinental layer (white curves).

Figure 2: Sketches of plume-lithosphere interactions. (a) a slow plume impinges on an elastic lithosphere, resulting in a single wavelength topographic signature; (b) when realistic mantle rheology is considered, and when rheological stratification of the lithosphere is accounted for, topographic undulations at the surface are to be expected.

Figure 3: Main external causes for the development of periodic or symmetric large-scale lithospheric undulations. In the first case (a), a compressive regime leads to lithospheric buckling/folding instabilities, resulting in long wavelength undulations of the lithosphere (two-dimensional topographic signature). In the second case (b), the arrival of a plume head results in similar signatures, but within a smaller domain (omni-directional 3D signature). Diagram (c) reveals the possible difficulty in distinguishing plume-induced from tectonically-induced topographic undulations.

Figure 4: Result of the numerical experiment on plume-lithosphere interaction beneath a continental lithosphere, where (1) realistic (brittle-elastic-ductile) mantle and crustal rheologies are considered, (2) rheological stratification of the lithosphere is accounted for, and (3) a free upper surface condition is

allowed. Details on the numerical set-up and procedure are explained in Burov and Guillou-Frottier (2005). The plume Rayleigh number equals 10^6 and surface topography shows different types of signature. The single wavelength is only obtained when the plume head is deep in the mantle and begins to rise (bottom). When plume head impinges on the lithosphere-astenosphere boundary, a subsidence phase is observed above plume head centre, as well as above each edge (top).

Figure 5: Map of Western Europe showing the surface topography, as available from GTOPO30, and location of the extracted topographic profiles. The east-west profiles crossing the Massif Central area (Profiles 1 to 13) are 650 km long. Other profiles (14 to 39) are 750 km long. The concentric profiles approximately follow large-scale topographic highs and lows induced by Alpine compression.

Figure 6: Smoothed topographic profiles over areas where mantle plumes are suggested. The right-hand column shows west-east profiles crossing the East African Rift system. In all four diagrams, a long wavelength component (grey dashed line) is superimposed with a short wavelength component (black dotted lines). Horizontal and vertical scales differ from one case to another.

Figure 7: Results from spectral (Fourier) analyses of topographic Profiles 1 to 26 (left) that include the French Massif Central and Paris Basin, and of topographic Profiles 27 to 39 (right) that include the Eifel area. Diamonds indicate the dominant-wavelength values identified in each spectrum. Symbol size is related to the amplitudes of each peak: the four symbol sizes increase according to the following ranges: 0-5%, 5-10%, 10-15%, and above 15% of the amplitude of the largest wavelength. The average dominant wavelength is outlined by a horizontal dashed line in both figures. Encircled areas show anomalous values and dotted lines suggest apparent spatial trends for certain groups of wavelengths (see text for discussion).

Figure 8: Analogy between topographic profiles obtained in numerical experiments on plume-lithosphere interactions (a-c), wavelet functions (d) and real topographic profiles (e) above the Massif Central (MC) and Eifeil (EiF) areas. Case (a) corresponds to unrealistic rheology and boundary conditions. Case (b) depicts the time-varying signature when realistic formulation of the lithosphere is accounted for (see Burov and Guillou-Frottier, 2005). Wavelets shown in (d) can be identified locally in real topographic profiles shown in (e).

Figure 9: Wavelet transforms of numerical topographic profiles computed for two distinct convective regimes: (a) the plume Rayleigh number Ra_p equals 10^6, and (b) Ra_p=5 10^6 (see Burov and Guillou-Frottier, 2005, for details on numerical experiments). From top to bottom: temperature field, surface topography and wavelet transforms are shown for four stages of transient evolution. "Mexican hat" and Morlet mother wavelets are used in both cases. See text for detailed comments.

Figure 10a: Topographic profiles (left column) located between the Massif Central (south) and the Eifel area (north), and their wavelet transforms (middle and right columns) with the "Mexican hat" (MH) and Morlet (MO) mother wavelets. Low- to medium-scale medium-energy coefficients are only identified in Profiles 17 and 18 (white ellipses). High-energy coefficients in the five profiles reveal horizontal wavelengths of ~200-250 km.

Figure 10b: Topographic Profile 52, bypassing topographic highs (top) and its wavelet transform with the "Mexican hat" mother wavelet in a 3D representation (bottom). Regular energy distribution is obtained over more than 1600 km. The apparent high-energy coefficients at the edges correspond to non-negligible border effects.

Figure 11: Arcuate topographic Profiles 53 and 54 (top) crossing both the Massif Central and the basins. 3D representation of wavelet scalograms obtained with the "Mexican hat" wavelet (bottom)

illustrate characteristic energy distribution in areas of supposed mantle plumes. Note that coefficient values are much higher than in Figure 10b. The Massif Central signature contains both large- and medium-scale high-energy coefficients, as do the Eifel and Sudetes areas. See detailed comments in text.

Figure 12: Series of east-west topographic profiles crossing the Massif Central from south (Profile 1) to north (Profile 12). Missing profiles (2, 4 and 13) have similar scalograms as their adjacent ones. The emergence of medium-scale high-energy coefficients (Profiles 7 to 11) resembles the case shown in Figure 9b.

Figure 13: Series of southeast-northwest topographic profiles crossing the Eifel-Ardennes area from southwest (Profile 28) to northeast (Profile 39). Missing profiles (27, 29 and 31) have similar scalograms as their adjacent ones. The emergence of medium-scale high-energy coefficients (Profiles 32 to 36) resembles the case shown in Figure 9b.

Figure 14: Series of south-north topographic profiles crossing the Bohemia-Sudetes area from west (Profile 22) to east (Profile 26). The emergence of medium-scale high-energy coefficients (white ellipses) tends to confirm the results from Profiles 53 and 54 (Figure 11).

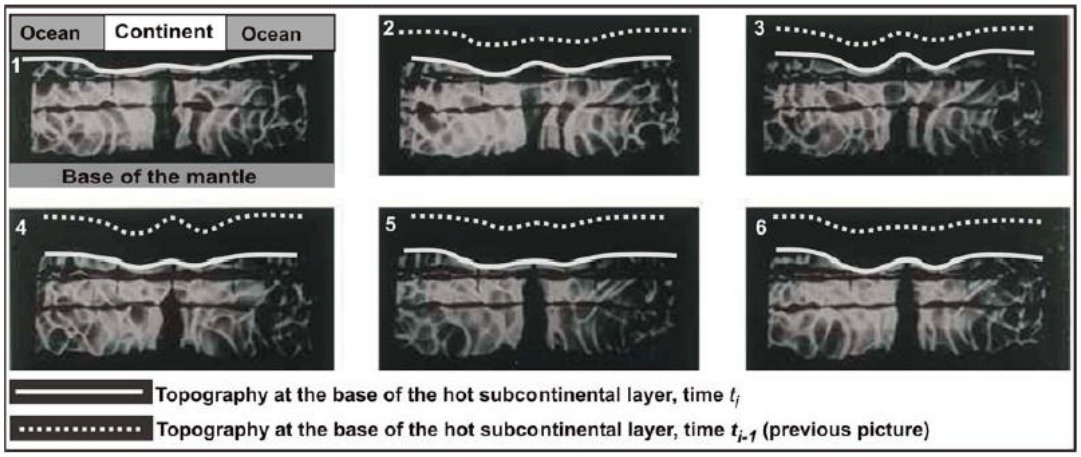

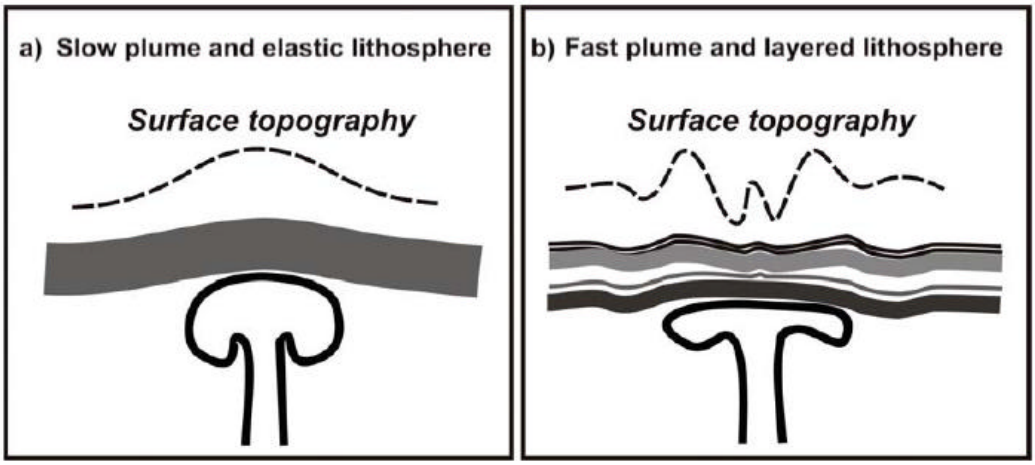

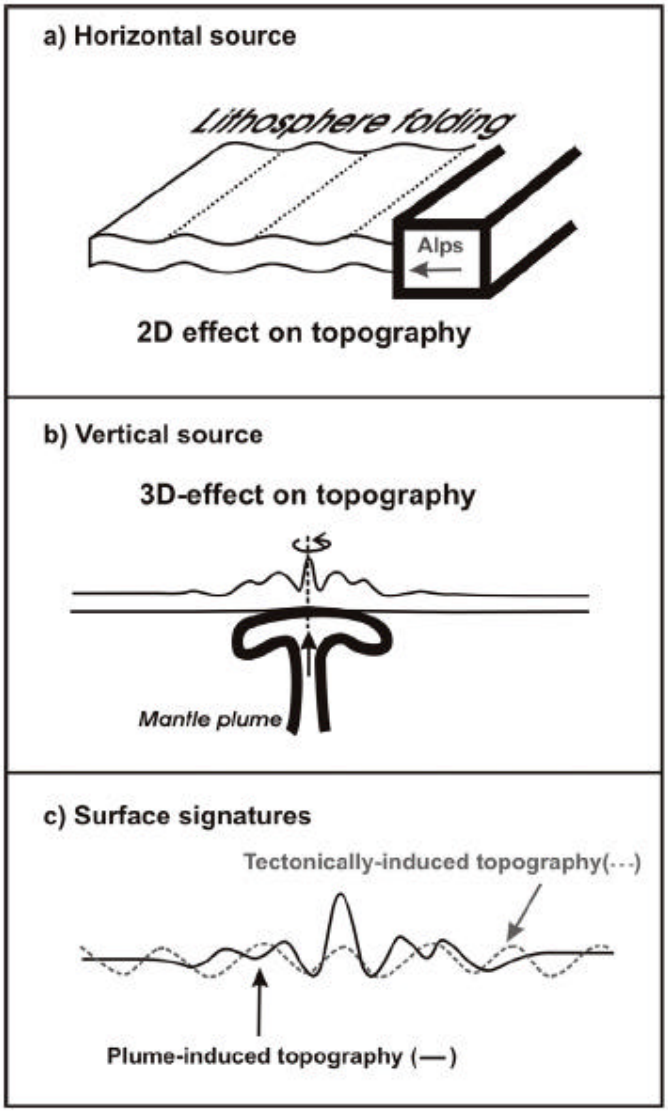

Figure 3

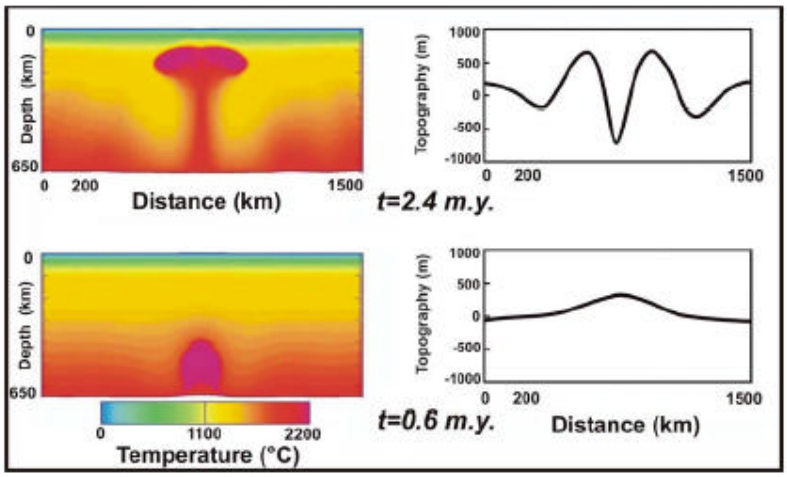

Figure 4

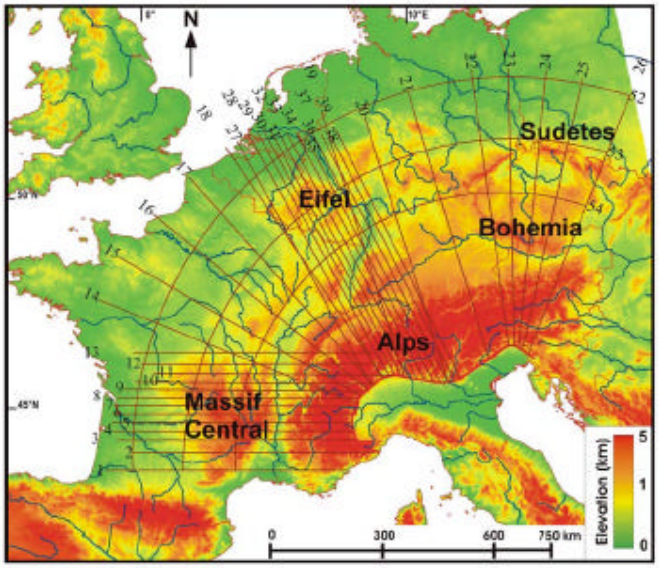

Figure 5

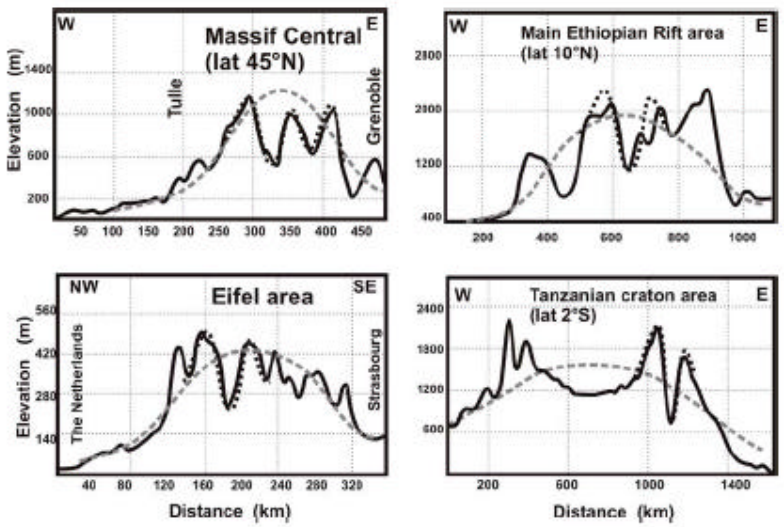

Figure 6

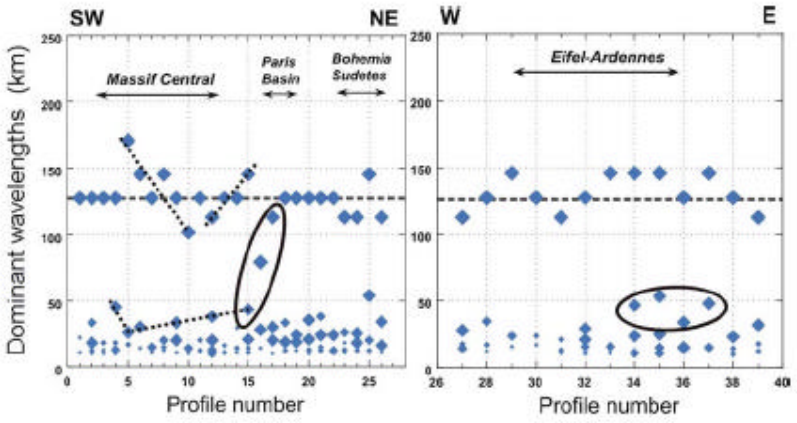

Figure 7

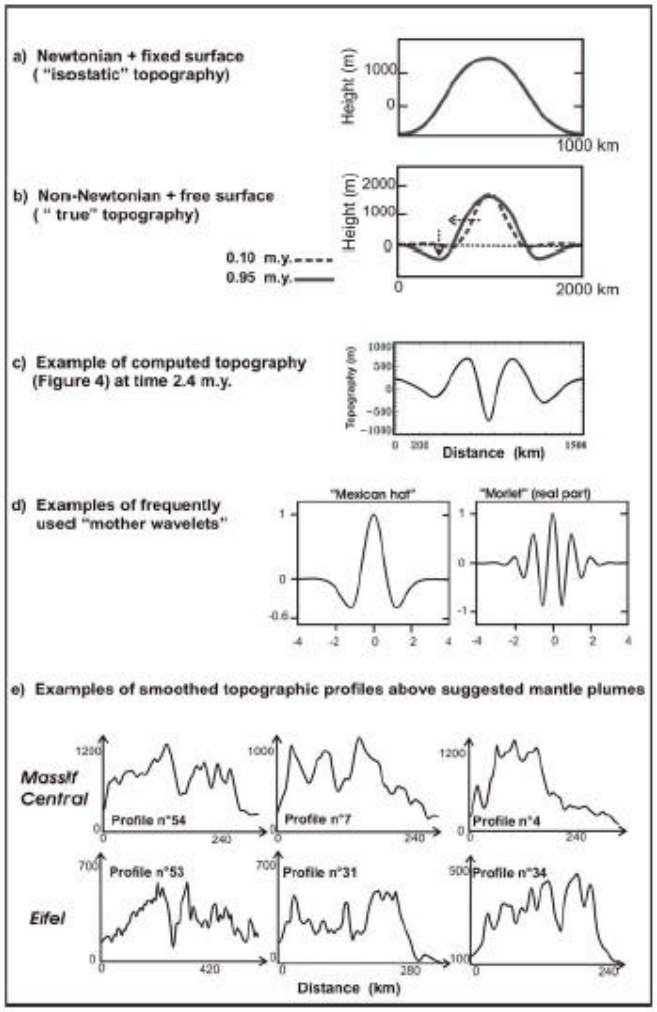

Figure 8

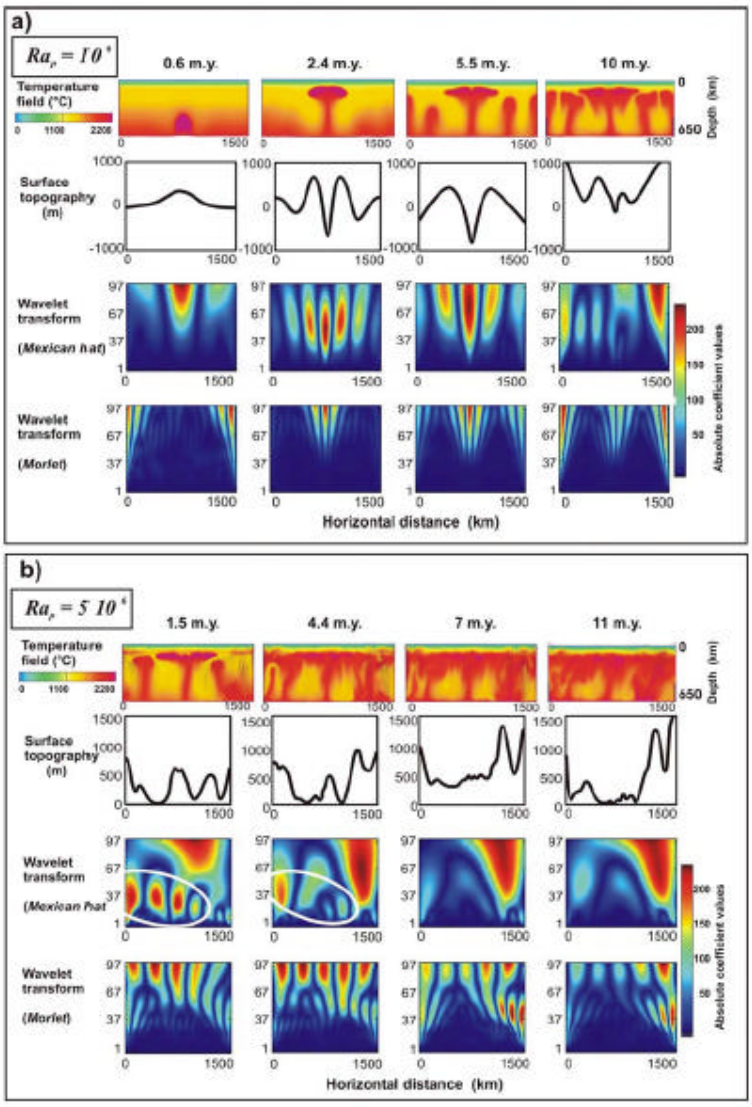

Figure 9

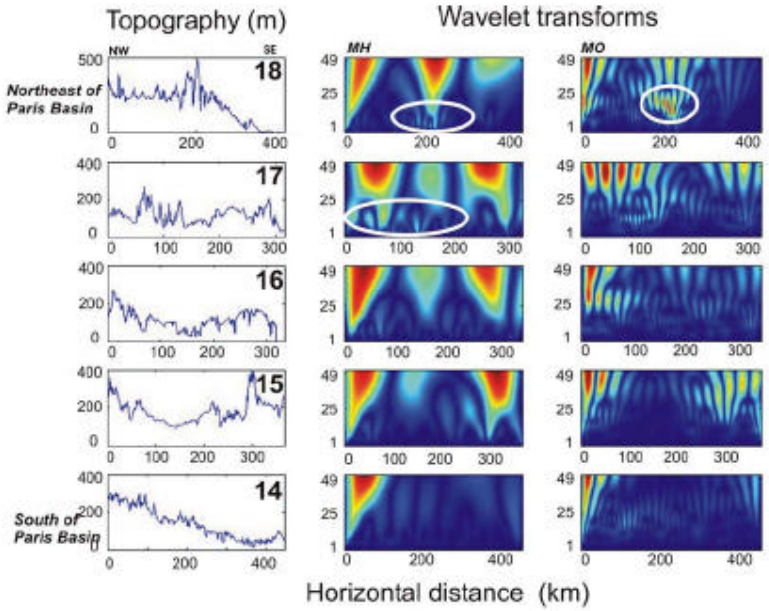

Figure 10a

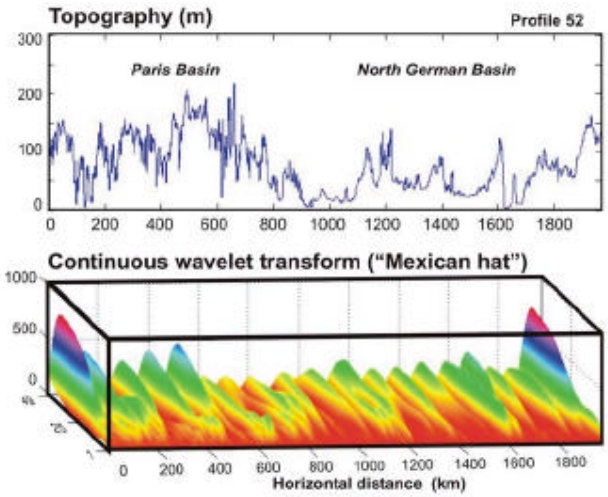

Figure 10b

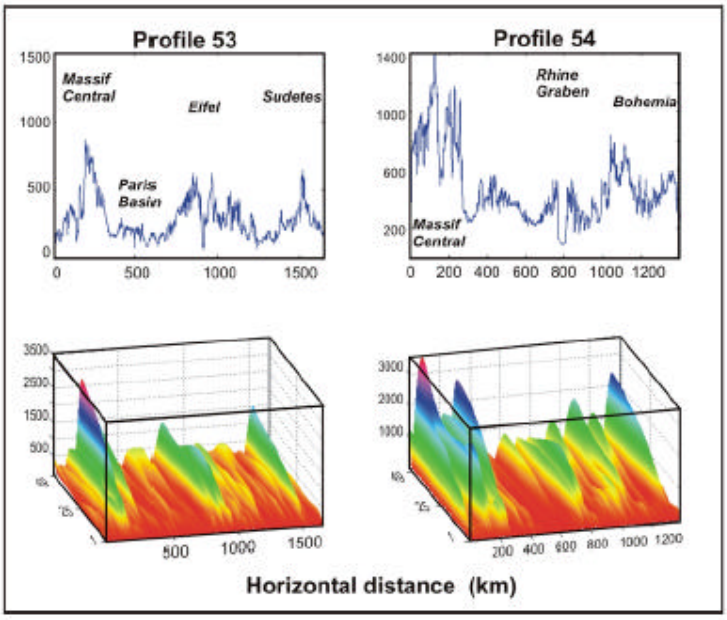

Figure 11

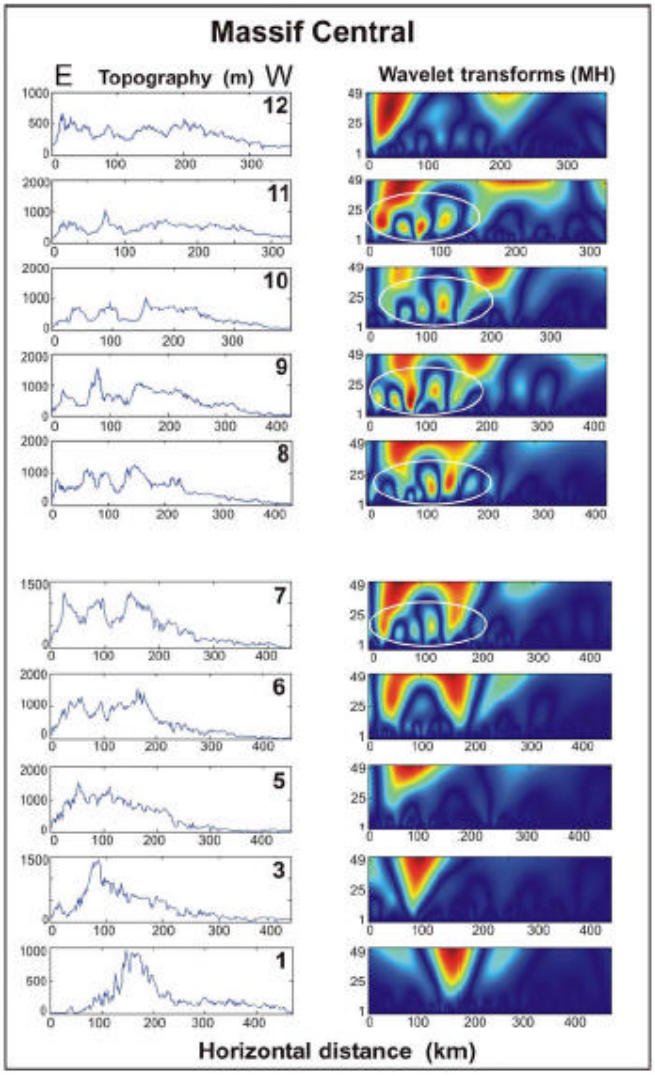

Figure 12

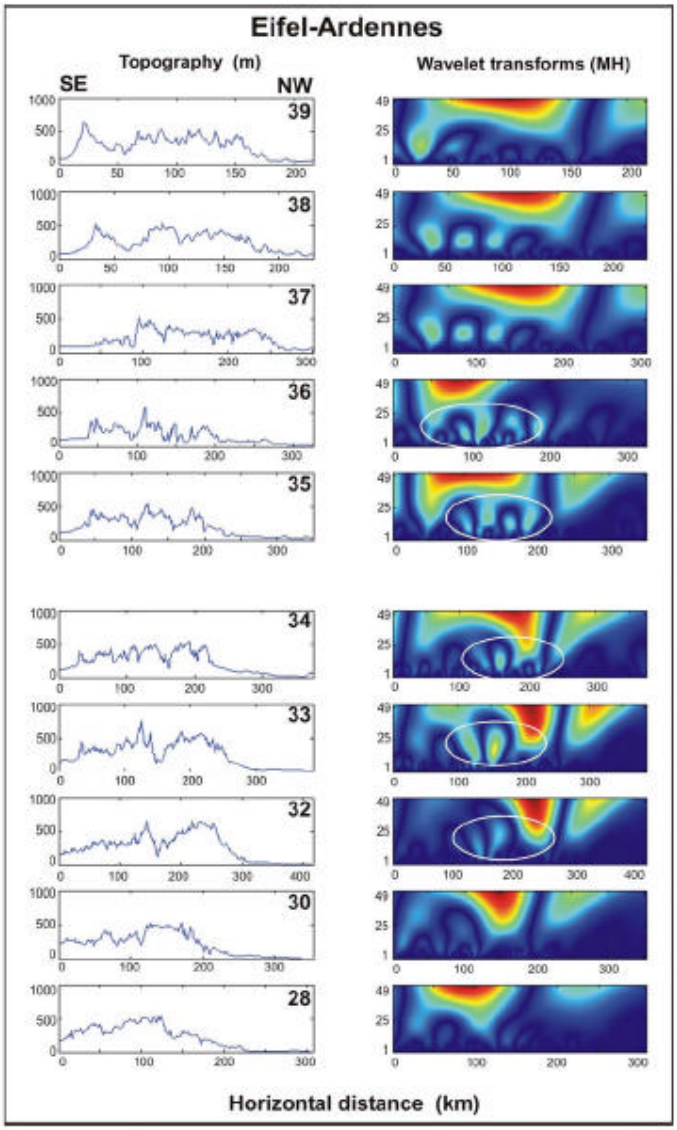

Figure 13

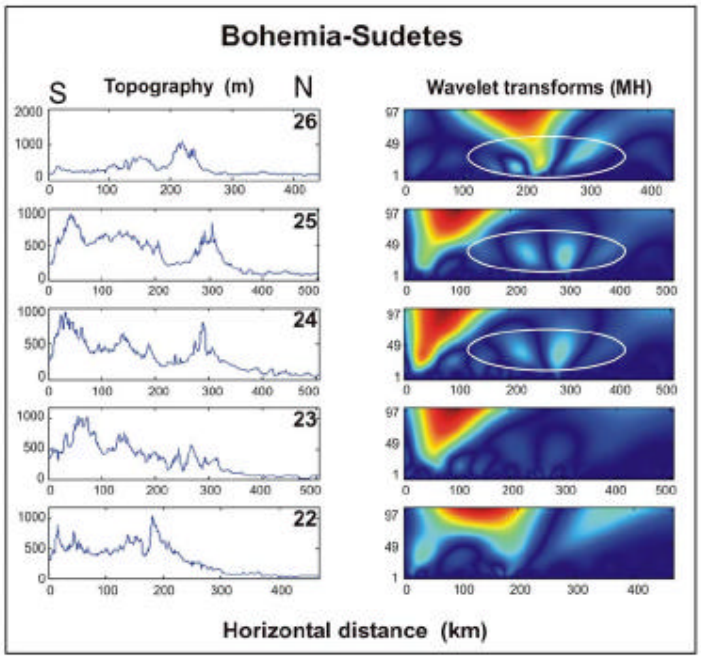

Figure 14